Neutrino oscillations at DUNE with improved energy reconstruction

Valentina De Romeri,[a,b] **Enrique Fernandez-Martinez**[a,b] **and Michel Sorel**[c]

[a] *Departamento de Física Teórica, Universidad Autónoma de Madrid,*
Cantoblanco E-28049 Madrid, Spain

[b] *Instituto de Física Teórica UAM/CSIC,*
Calle Nicolás Cabrera 13-15, Cantoblanco E-28049 Madrid, Spain

[c] *Instituto de Física Corpuscular (IFIC), CSIC and Universitat de Valencia,*
Calle Catedrático José Beltrán, 2, 46980 Paterna, Valencia, Spain

E-mail: valentina.deromeri@uam.es, enrique.fernandez-martinez@uam.es,
sorel@ific.uv.es

Abstract: We study the physics reach of the long-baseline oscillation analysis of the DUNE experiment when realistic simulations are used to estimate its neutrino energy reconstruction capabilities. Our studies indicate that significant improvements in energy resolution compared to what is customarily assumed are plausible. This improved energy resolution can increase the sensitivity to leptonic CP violation in two ways. On the one hand, the CP-violating term in the oscillation probability has a characteristic energy dependence that can be better reproduced. On the other hand, the second oscillation maximum, especially sensitive to $\delta_{\rm CP}$, is better reconstructed. These effects lead to a significant improvement in the fraction of values of $\delta_{\rm CP}$ for which a 5σ discovery of leptonic CP-violation would be possible. The precision of the $\delta_{\rm CP}$ measurement could also be greatly enhanced, with a reduction of the maximum uncertainties from 26° to 18° for a 300 MW·kt·yr exposure. We therefore believe that this potential gain in physics reach merits further investigations of the detector performance achievable in DUNE.

Contents

1 Introduction

The experimental evidence for neutrino flavor change from the neutrino oscillation phe-
nomenon can be explained consistently through three family mixing encoded in the uni-
tary Pontecorvo-Maki-Nakagawa-Sakata (PMNS) matrix [1–5] in perfect analogy to the
CKM matrix in the quark sector. However, the actual measurements of its elements re-
veal a structure completely different to its quark counterpart, increasing the complexity
and mystery of the Standard Model (SM) flavor puzzle. Indeed, far from the hierarchi-
cal structure characterized by very small mixings of the CKM, large mixing angles are
required to describe lepton mixing through the PMNS matrix. While the "solar" mix-
ing angle has been measured to be $\theta_{12} \sim 33.5°$, the "atmospheric" mixing angle θ_{23} is
compatible with maximal mixing [6]. The discovery of a non-zero and relatively large
θ_{13} mixing angle, $\theta_{13} \sim 8.5°$ [7–11] now opens the window to the precision era in the
measurements of the PMNS elements and to explore the existence of leptonic CP viola-
tion at present and near future oscillation facilities. Furthermore, the Jarlskog invariant
$J = 1/8 \cos\theta_{13} \sin 2\theta_{13} \sin 2\theta_{12} \sin 2\theta_{23} \sin \delta_{\rm CP}$, which encodes the amount of CP violation
present in the mixing matrix, can be potentially as large as ~ 0.035 for maximally CP vi-
olating values of $\delta_{\rm CP}$, three orders of magnitude larger than the value of its counterpart in
the quark sector: $J_{\rm CKM} = (2.96^{+0.20}_{-0.16}) \times 10^{-5}$ [12]. Since it has been shown that, within the
context of Standard Model Electroweak Baryogenesis, $J_{\rm CKM}$ is not large enough to account
for the observed Baryon Asymmetry of the Universe [13, 14], the discovery of an additional

source of CP violation (such as δ_{CP} in the PMNS matrix) would be a very welcome input to tackle this open problem of the SM.

At present, T2K [15] and NOνA [16] are providing the first tantalizing hints for maximal leptonic CP violation $\delta_{CP} \sim -90°$ when combined with reactor neutrino results. While the actual significance of these hints is still low [6, 17, 18], they at least lead to a consistent picture. Nevertheless, a new generation of neutrino oscillation facilities, characterized by intense beams and large detectors, will be required to definitely settle the issue. These facilities will also unveil other present unknowns, such as the octant of θ_{23}, if it turns out not to be maximal, and the neutrino mass hierarchy. Both these measurements have deep consequences in our understanding of the flavor puzzle. Indeed, deviations of θ_{23} from maximality can be crucial to understand if the observed flavor structure stems from a deeper underlying symmetry structure. The ordering of the neutrino mass eigenstates will reveal whether the spectrum is similar to that of quarks (with the lighter states having a larger mixing with the lighter charged lepton: the electron) for a normal hierarchy (NH) or opposite in that sense, for inverted (IH). The hierarchy determination is also a crucial input to neutrinoless double beta decay searches probing the Majorana nature of the neutrino fields. If neutrinos do indeed turn out to be Majorana particles, this would imply violation of lepton number and could again hint at a neutrino explanation of the observed Baryon Asymmetry of the Universe via the leptogenesis [19] mechanism.

In this work, we re-evaluate the physics potential to address these unknowns of the proposed DUNE [20] experiment exploiting the prospective LBNF facility at Fermilab. In particular, we analyze the energy reconstruction capabilities of the proposed liquid Argon (LAr) far detector and, with them, compute the physics reach of the experiment on the mass hierarchy, the octant of θ_{23} and the discovery of leptonic CP violation. In section 2 we discuss the simulations performed to characterize the energy reconstruction capabilities of the DUNE far detector. In section 3 we describe the experimental setup considered. In section 4 we analyze the sensitivity of the facility to the different physical observables in view of the previous results. Finally in section 5 we draw our conclusions and summarize our results.

2 Neutrino energy reconstruction

In a neutrino detector, the energy of an incoming neutrino undergoing a charged-current (CC) interaction can be reconstructed either using charged lepton kinematics only (kinematic or quasi-elastic method), or using the entire visible energy in the event (calorimetric method), see for example [21, 22]. For neutrino beams extending into the multi-GeV energy regime, as in the DUNE case, inelastic interactions are dominant and the calorimetric method is usually preferred. The performance of calorimetric neutrino energy reconstruction has been studied in detail in the context of the MINOS [23] and NOνA [24] experiments. For LAr-TPC neutrino detectors, studies primarily based on simulations exist, see for example [20–22, 25–28]. Ongoing and planned efforts relying on LAr-TPCs exposed to charged particle [29–31] and neutron [32] test beams are expected to provide additional calibration data for energy reconstruction purposes in the near future. In general, the calorimetric energy reconstruction of neutrino interactions in a LAr-TPC is expected to be driven by event-by-event fluctuations in the effects listed in table 1 [21, 27].

Number	Description
1	Nuclear effects in neutrino interactions
2	Non-deposited energy carried away by neutrinos
3	Particle (other than neutrino) leakage out of the active volume
4	Quenching of LAr ionisation/excitation from nuclear fragments
5	Electron-ion recombination
6	Electron attachment along drift
7	Electronic noise of the charge read-out system

Table 1. Effects affecting calorimetric neutrino energy reconstruction in LAr-TPCs.

In this work, we adopt a simple approach to energy reconstruction, extending the studies of ref. [21]. We use detailed simulations of neutrino interactions and LAr response in a DUNE far detector module full geometry. We predict the total yield N_e of ionisation electrons per event produced in the LAr active volume, for neutrino CC interactions of all relevant neutrino flavors and energies. We use N_e as our estimator for the incoming neutrino energy E_ν, and hence event-by-event fluctuations in N_e to estimate the DUNE far detector energy resolution performance. In our approach, we do not attempt to identify final state particles or neutrino interaction types. The full event charge produced in the LAr active volume is simply summed together, regardless of the final state particles producing it, and regardless of the time delay or spatial separation from the neutrino interaction vertex. In other words, we fully account for effects 1 to 5 in table 1. We neglect electron attachment along drift (item 6) and electronic noise (item 7) contributions. The impact of these two items on calorimetric neutrino energy reconstruction depends on the details of the LAr-TPC detector under consideration, particularly on the LAr purity and the electronic noise levels. Their impact also depends on the actual reconstruction algorithms used, such as the hit finding algorithm to identify the read-out elements (wires or strips) and time samples carrying non-zero charge information, and the charge attenuation correction as a function of drift length. In the following, we assume that these effects have a negligible effect on calorimetric energy resolution compared to the other sources in table 1. This is a plausible assumption, if we consider the impact of LAr-TPC full reconstruction effects obtained from earlier studies with simpler (non-neutrino) event topologies. In particular, ICARUS inferred a resolution of $\Delta E/E = 1.0\%/\sqrt{E~(\text{GeV})}+1.2\%$ for electromagnetic showers induced by 0.05–5 GeV single photons [33]. As we will see, contributions at this level would be negligible compared to the neutrino energy resolutions we obtain.

We note that our simple approach to calorimetric neutrino energy reconstruction could be refined, potentially yielding better energy resolutions than the ones presented here. Particle or event identification could be exploited for calorimetry, thanks to known differences in detector response for different particles or events. In addition, scintillation light information may provide an additional handle to improve calorimetric energy resolution, as discussed in [21].

In the following, we discuss our energy reconstruction results for CC neutrino interactions (section 2.1), how our strategy and results compare with previous studies (section 2.2), and how we treat energy reconstruction for neutral-current (NC) neutrino interactions (section 2.3).

2.1 LArSoft studies for charged-current neutrino interactions

We use the LArSoft code ([34], version v04_09_00) for our energy reconstruction studies. LArSoft is the software framework for simulation and reconstruction adopted by all LAr neutrino experiments, DUNE included. In particular, we use LArSoft for the detector geometry description, the simulation of neutrino-argon interactions, the propagation of final state particles in the detector active volume and surroundings, and for the description of the resulting ionization yields. We discuss each one of these aspects below.

The LAr-TPC detector geometry description used in LArSoft corresponds to one of the four far detector modules for DUNE at the Sanford Underground Research Facility (SURF). This geometry, in GDML format, has been provided to us by the DUNE Collaboration. It is equivalent to the "workspace" GDML geometries provided in [35], with the exception that it describes the full, 17 kt total LAr mass, detector module as opposed to only part of it. The detector enclosure, cryostat, 300 TPCs envisaged within the detector module, and the anode/cathode plane assemblies, are simulated. We do not consider readout effects in our studies, and hence we make use of the geometry description that does not include LAr-TPC wires, as discussed in [35]. The dimensions of the LAr active volume extend from -7.46 m to +7.46 m in the X direction, from -6.08 m to +6.08 m in the Y direction, and from 0 to +58.1 m in the Z direction. The coordinate system convention adopted is such that Z is the beam direction and pointing downstream of the detector, Y is the vertical direction and pointing up, and the TPC drift direction X is taken to form a right-handed coordinate system.

Neutrino-argon interactions are generated uniformly in the full LAr active volume using LArSoft, which in turn relies on the GENIE event generator code, version 2.8.6 [36]. Our energy resolution studies assume mono-energetic neutrinos of ν_e, $\bar{\nu}_e$, ν_μ, $\bar{\nu}_\mu$ flavors, stepping through the relevant 0.25–10 GeV neutrino energy range. GENIE accounts for a comprehensive list of quasi-elastic, resonant, deep inelastic and coherent CC interaction channels. Nuclear effects, affecting both the initial and the final state of the interaction, are also accounted for.

All particles present in the neutrino-argon interaction final state are then propagated in LAr using the GEANT4-based [37] detector simulation in LArSoft. The simulation uses the QGSP_BERT physics list [38], using a Bertini cascade model for hadrons of energy below ~10 GeV. The list contains all standard electromagnetic and weak decay processes. Compared to the default LArSoft physics list, we disable the neutron tracking cut, as in [21], to track neutrons down to thermal energies.

Charged particles deposit energy by ionizing and exciting argon atoms, ultimately producing charge and light signals to be detected at readout planes. The simulation of charge and scintillation light signals is performed via the NEST [39] model, as in [21]. The model accounts for quenching of LAr ionisation/excitation from nuclear fragments because of dissipation in the form of heat, and for electron-ion recombination. For the latter, a modified Birks' formula [40] and a 0.5 kV/cm drift field are assumed. We have verified that our energy reconstruction results are nearly insensitive to the details of the ionisation model chosen, with similar results obtained using the LArSoft default model [34] compared to the more detailed NEST model [39].

For our energy reconstruction studies, we assume the following fiducial volume definition (numbers in meters): [-6.5,-0.5]∪[+0.5,+6.5] in X, [-5.0,+5.0] in Y, [+1.0,+54.0] in Z,
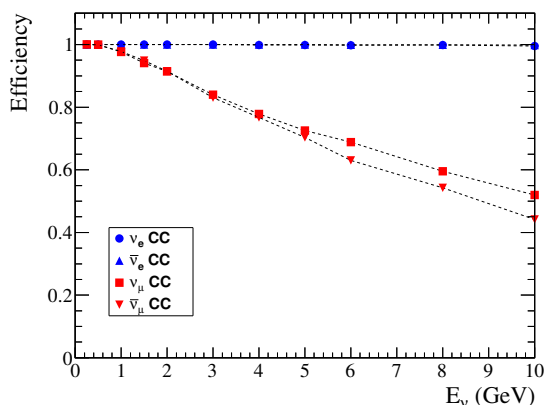
Figure 1. Expected efficiency to fully contain the primary lepton within the LAr active volume, for ν_e, $\bar{\nu}_e$, ν_μ and $\bar{\nu}_\mu$ CC interactions in the LAr fiducial volume. The efficiency is shown as a function of neutrino energy.

for a LAr fiducial mass per detector module of about 9 kt. This fiducial mass is similar to the 10 kt value assumed in the DUNE CDR [20]. The gap in the fiducial volume near X=0 is due to the anode plane assembly. Our fiducial volume selection has been chosen by requiring an approximately constant average deposited energy as a function of (X,Y,Z) for relatively high energy (6 GeV) ν_e CC events, where the coordinates indicate the neutrino interaction location. Interactions occurring outside the fiducial volume are characterized by a rapidly decreasing average deposited energy, because of increased particle leakage out of the LAr volume. In this outer region, the detector would therefore have diminished neutrino energy reconstruction capabilities.

In addition to this fiducial volume requirement, we only select neutrino CC interactions where the primary lepton (that is, the charged lepton produced at the neutrino CC interaction vertex) is fully contained within the LAr active volume. This is motivated by the desire of obtaining the best possible neutrino energy resolution. The efficiencies for primary lepton containment are shown in figure 1. While the lepton containment efficiency is 100% for fiducial ν_e and $\bar{\nu}_e$ CC interactions at all relevant energies, the efficiency decreases with neutrino energy for ν_μ and $\bar{\nu}_\mu$ CC interactions, as expected. However, even for 6 GeV ν_μ and $\bar{\nu}_\mu$ CC, the efficiency is greater than 60%.

As mentioned above, we use the total ionization charge produced in the LAr active volume per neutrino interaction, N_e, as our estimator for the incoming neutrino energy E_ν. The left panel of figure 2 shows the N_e/E_ν distribution for 4 GeV ν_e CC interactions in the DUNE fiducial volume as an example. On average, about 30 electron-ion pairs per keV of neutrino energy are produced. This number is significantly smaller than the 42 electrons/keV value expected from the ionization yield in LAr [41]. The difference is due to the detection effects mentioned above, particularly electron-ion recombination. These same effects (items 1–5 in table 1) are also responsible for the event-by-event fluctuations in N_e/E_ν. We estimate the neutrino energy resolution as the RMS width of N_e/E_ν distributions such as the one in the left panel of figure 2.

The relative neutrino energy resolution for ν_e, $\bar{\nu}_e$, ν_μ, $\bar{\nu}_\mu$ CC interactions and as a function of neutrino energy obtained from this procedure is shown in the right panel of
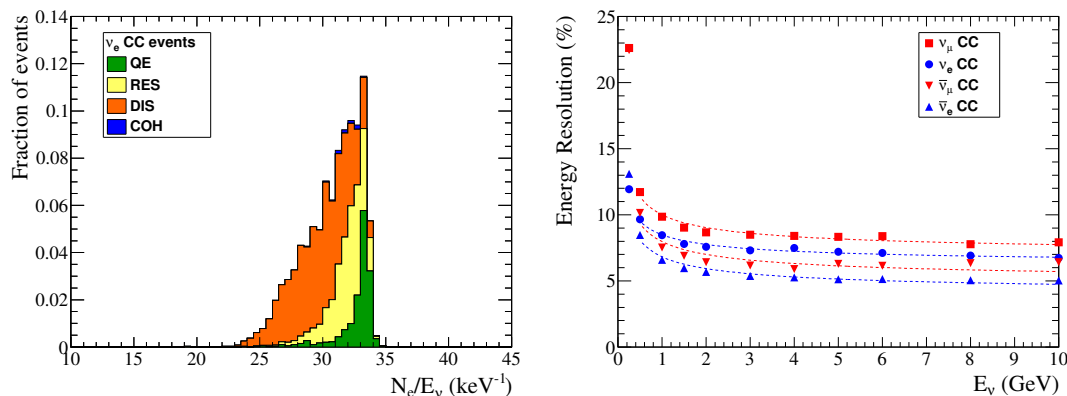
Figure 2. Left panel: number of ionization electrons N_e produced in the LAr active volume per incoming neutrino energy E_ν, for 4 GeV ν_e CC interactions throughout the LAr fiducial volume. The colors indicate different interaction types: quasi-elastic scattering (QE), resonant interactions (RES), deep inelastic scattering (DIS) and coherent pion production interactions (COH). Right panel: neutrino energy resolution expected from our LArSoft simulations and as a function of neutrino energy, for ν_e, $\bar{\nu}_e$, ν_μ and $\bar{\nu}_\mu$ CC interactions. The dashed lines correspond to the parametrizations given in the text.

figure 2. From the figure, energy resolutions of order 10% or better are expected, with only a mild dependence on neutrino flavor or neutrino energy. For our physics studies, we parametrize the neutrino energy resolution via gaussian functions with flavor- and energy-dependent widths given by:

$$\nu_e \text{ CC:} \qquad \Delta E_\nu/E_\nu = 0.060 + 0.025/\sqrt{E_\nu} \tag{2.1}$$

$$\nu_\mu \text{ CC:} \qquad \Delta E_\nu/E_\nu = 0.067 + 0.033/\sqrt{E_\nu} \tag{2.2}$$

$$\bar{\nu}_e \text{ CC:} \qquad \Delta E_\nu/E_\nu = 0.038 + 0.030/\sqrt{E_\nu} \tag{2.3}$$

$$\bar{\nu}_\mu \text{ CC:} \qquad \Delta E_\nu/E_\nu = 0.047 + 0.033/\sqrt{E_\nu} \tag{2.4}$$

where the neutrino energy E_ν is expressed in GeV. The parametrizations in eqs. (2.1)–(2.4), also shown in figure 2 as dashed lines, are obtained by fitting our LArSoft energy resolution results in the 0.5–10 GeV energy range.

The importance of DUNE's neutron detection capabilities for calorimetric neutrino energy reconstruction is illustrated in figure 3. The left panel of figure 3 shows average ionization yields per unit neutrino energy, $\langle N_e/E_\nu \rangle$, as a function of energy and for two different neutron detection assumptions. In both cases, only the ionization signals created as a result of neutron interactions in LAr are considered as neutron visible energy. The higher ionization yield assumes that all neutron-induced ionization in the LAr active volume can be detected, regardless of the delay or distance from the neutrino interaction time or vertex. The lower yield assumes that only the prompt neutron visible energy is detected, where prompt is defined as occurring within 10 μs from the neutrino interaction. For both assumptions, we find that $\langle N_e/E_\nu \rangle$ is stable to within $\simeq$2% over the entire neutrino energy range of relevance for DUNE. Our simulations thus confirm that the total charge produced in the LAr is a good neutrino energy estimator. A larger effect is seen on the overall energy scale, with the less efficient neutron detection scenario collecting approximately 15% less
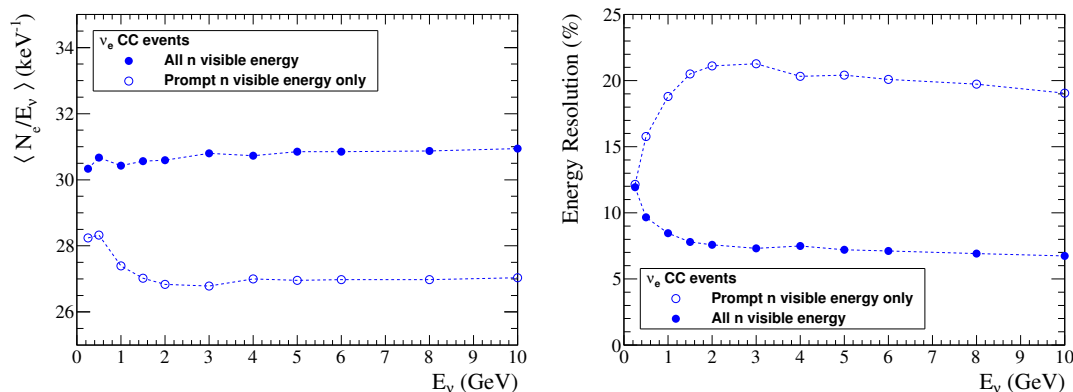
Figure 3. Average energy scale parameter $\langle N_e/E_\nu \rangle$ (left) and neutrino energy resolution (right) versus E_ν for fiducial ν_e CC events, for two different assumptions concerning DUNE neutron detection capabilities (see text for details).

charge. While our work focuses on neutrino energy resolution, the left panel of figure 3 also gives us some indications on the scale of possible neutrino energy reconstruction biases in DUNE. Energy-scale uncertainties can affect long-baseline oscillation sensitivities [20] and, if not properly accounted for, can even introduce biases in the extracted oscillation parameters such as δ_{CP} [28]. In the context of our calorimetric neutrino energy reconstruction, biases can occur either through a non-linear N_e response as a function of neutrino energy, or through an overall shift of the energy scale parameter $\langle N_e/E_\nu \rangle$. The left panel of figure 3 suggests that inefficient detection and mis-modelling of neutrons may contribute significantly to neutrino energy reconsruction biases, and therefore requires dedicated efforts in neutron simulation, reconstruction and calibration campaigns.

The right panel of figure 3 shows the neutrino energy resolution as a function of neutrino energy for fiducial ν_e CC events for the same two cases, namely the detection of all neutron-induced visible energy, or the detection of only its prompt ($<10~\mu$s) component. The latter assumption yields a neutrino energy resolution that is more than a factor of two worse than the former assumption, across all relevant neutrino energies. It is therefore clear that neutron detection plays a major role for accurate calorimetric neutrino energy resolution in DUNE.

In the following, we assume the more efficient neutron detection scenario for our studies. This is because the DUNE readout times per event will be at least 2.25 ms [42], far larger than the 10 μs detection time window considered in the other scenario. While closer to reality, our assumption may be somewhat too optimistic, considering that neutron thermalization times are also $\mathcal{O}(1~\text{ms})$ and that the hit finding algorithm for neutron-induced isolated hits may not be perfectly efficient.

2.2 Comparison with DUNE CDR assumptions

The energy resolution functions for ν_e, $\bar{\nu}_e$, ν_μ, $\bar{\nu}_\mu$ CC interactions obtained in section 2.1 can be compared with the assumptions made in the DUNE CDR [20] and in other physics studies [22, 43]. These studies rely on a different strategy to evaluate the neutrino energy resolution compared to ours. Full simulations are employed only to evaluate nuclear effects

in neutrino interactions (item 1 in table 1), but not for the LAr-TPC detector response. Rather, a parametrized response for each single particle emerging from the target nucleus is typically applied to account for all other effects (items 2–7 in table 1). These parametrizations introduce single-particle energy and angular smearing, single-particle energy thresholds for detection and single-particle energy reconstruction biases. The parametrizations are informed from GEANT4 [37] particle trajectories in liquid argon, by detector response simulation studies in other LAr-TPCs, by results reported by the ICARUS Collaboration, and by the expected DUNE far detector geometry, see [20, 43] for details. The single-particle detector responses are then combined to estimate the reconstruction performance for event-level kinematic quantities such as the incoming neutrino energy.

In LBNE studies [43], the ν_e energy resolution value is assumed to be dominated by the hadronic shower resolution. The latter is taken to be $30\%/\sqrt{E}$, where the hadronic energy E is expressed in GeV, and hadrons are assumed to carry a 40% fraction of the total event energy on average. As a result, LBNE physics studies assume a $15\%/\sqrt{E_\nu}$ resolution for ν_e CC interactions of energy E_ν. For ν_μ CC interactions, LBNE studies further assume a 10–15% resolution for partially contained muons, to be added to the hadronic shower resolution contribution, resulting in a $20\%/\sqrt{E_\nu}$ resolution overall for ν_μ CC interactions.

The DUNE CDR [20] adopts a more sophisticated, Fast MC-based, approach compared to LBNE studies. A different resolution function is assumed for several final state particle categories: muons, charged pions, electrons or gammas, protons, neutrons, and other particles. For exiting particles, the particle energy is smeared according to deposited (and not total) energy. A bias in the energy reconstruction of neutrons is also considered, with only 60% of the neutron deposited energy assumed to be reconstructed on average. Furthermore, low-energy ($<1\,\mathrm{GeV}/c$) neutrons are considered to have a 10% chance to remain undetected.

In the work by Ankowski et al. [22], all neutrons are assumed to escape detection. Two scenarios are considered. In the so-called *perfect reconstruction*, all particles (except neutrons) exiting the target nucleus are observed, and their measured energies are equal to the true ones. In the *realistic reconstruction*, the measured energies and angles are smeared to account for detector resolution effects, and single-particle detection efficiencies and energy thresholds are taken into account. We consider both scenarios in our comparison.

The LBNE, DUNE CDR and Ankowski et al. assumptions for ν_e and ν_μ CC interactions are shown in figure 4, together with our LArSoft-based results. Significant differences in energy resolution assumptions exist between LBNE and DUNE CDR studies, the latter being significantly more conservative. For example, for $1\,\mathrm{GeV}$ ν_e CC interactions, LBNE studies assume a 15% resolution, while the DUNE CDR about 35% (see left panel of figure 4). Also, our detailed simulations indicate a largely improved energy resolution at all energies compared to the DUNE CDR, and also a better resolution compared to LBNE at low energies. For example, for the same case of $1\,\mathrm{GeV}$ ν_e CC interactions, we expect about a 8.5% resolution, that is about a factor of 4 better than DUNE CDR assumptions. Large improvements exist also in the ν_μ CC case. Finally, our neutrino energy resolutions are also significantly better than the calorimetric resolutions obtained by Ankowski et al...

In order to take full advantage of these improved energy resolution assumptions, in our oscillation analysis we choose $50\,\mathrm{MeV}$ wide bins in reconstructed neutrino energy. This is to be compared with the $125\,\mathrm{MeV}$ wide bins considered in the DUNE CDR studies.
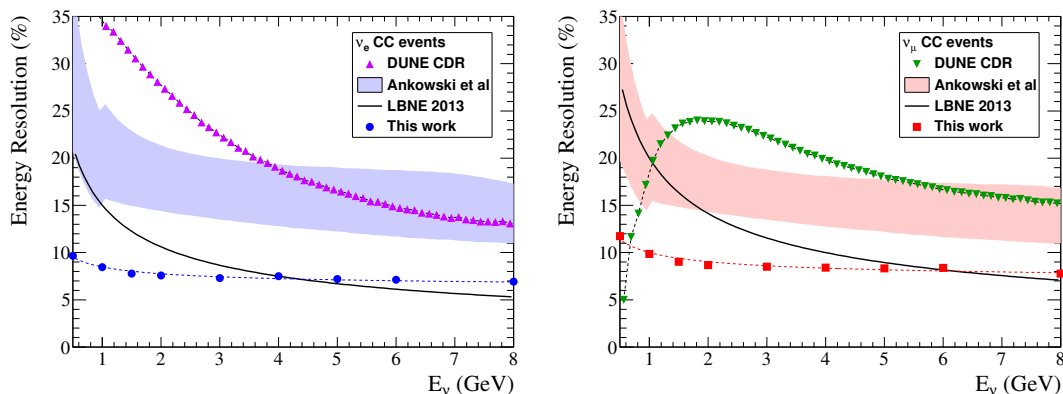
Figure 4. Neutrino energy resolution as a function of neutrino energy, for ν_e (left panel) and ν_μ (right) CC interactions. Expectations from our LArSoft-based studies are shown for fiducial neutrino interactions with fully contained primary leptons. For comparison, the solid curves are the resolution functions assumed in LBNE sensitivity studies [43], the triangular markers are the DUNE CDR [20] assumptions, and the filled bands are the results obtained by Ankowski et al. [22]. For the Ankowski et al. results, the lower limit corresponds to the perfect reconstruction case, and the upper limit to the realistic reconstruction scenario.

2.3 Neutral-current neutrino interactions

Neutral-current interactions can constitute a background for ν_e appearance and ν_μ disappearance searches in DUNE. For this reason, energy reconstruction studies have been performed for NC interactions as well. In the NC case, a simple gaussian smearing of true to reconstructed neutrino energy is a poor approximation, given that the outgoing neutrino carries a large fraction of the event energy. In this case, we use a more general approach. For a given true neutrino energy, the probability to obtain a reconstructed neutrino energy value is encoded in a matrix form, by using the distribution of deposited energies expected from neutrino NC interactions occurring throughout the LAr fiducial volume. Since the dominant effect on energy resolution is given in this case by non-deposited energy carried away by neutrinos, we neglect in the NC case fluctuations associated with the ionisation yield modelling and consider only items 1–3 in table 1.

Our LArSoft-based results for neutrino and anti-neutrino NC interactions are shown separately in the left and right panels of figure 5. We use the smearing matrices in figure 5 to compute the NC background event rates in our 50 MeV wide bin analysis. We have verified that these smearing matrices give comparable background rates with respect to the NC smearing assumed in the DUNE CDR [20], when the same 125 MeV wide bins in reconstructed neutrino energy are used for both.

3 Experimental setup

We use the neutrino energy reconstruction results of section 2 as input to our long-baseline neutrino oscillation physics studies. We use the GLoBES software ([44, 45], version 3.2.16) to describe the experiment and to extract oscillation sensitivities. All experimental assumptions used in our GLoBES description are given in section 3.1. The resulting event rates and energy spectra are presented in section 3.2.
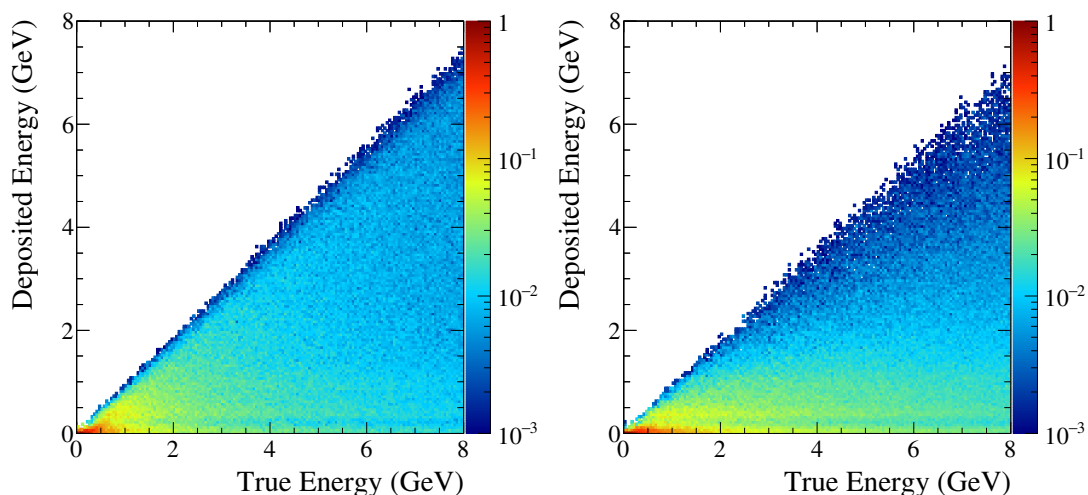
Figure 5. The expected energy smearing matrix for ν_μ NC (left) and $\bar{\nu}_\mu$ NC (right) interactions occurring in the LAr fiducial volume. The deposited (true) neutrino energy is shown in the vertical (horizontal) axes, respectively.

3.1 GLoBES description

Our framework to describe the DUNE experimental setup starts from the same assumptions used in the DUNE CDR [20], which is also GLoBES-based. The experiment simulation configurations used in the DUNE CDR are described in detail in, and are publicly available at [35]. The experimental setup is thus only summarized in the following. We depart from the DUNE official description only for aspects related to neutrino energy reconstruction (the aspect we wish to address in this work) and event selection efficiencies.

The neutrino flux assumptions are the same as in the DUNE CDR [20]. They were produced with the G4LBNF Geant4-based [37] simulation of the LBNF beamline. We use the "optimized" beam design in [35] for our studies. The optimized design provides a significantly higher neutrino flux near the second oscillation maximum compared to the "reference" design. In order to account for Earth matter effects on neutrino propagation, we use a constant matter density profile from [46, 47].

We assume a LAr detector fiducial mass of 40 kt, as in the DUNE CDR [20]. This fiducial target mass corresponds to four detector modules with 10 kt fiducial mass each. Overall, we assume an exposure of 150 MW·kt·yr in neutrino (forward horn current, FHC) running mode, and the same exposure for anti-neutrino (reverse horn current, RHC) running mode. Given the beam power (1.07 MW) and detector fiducial mass (40 kt) assumptions, these numbers correspond to about 3.5 years of FHC beam, plus 3.5 years of RHC beam [35].

Neutrino-argon interaction cross-sections in tabulated form are also taken from [35]. The cross-section files are generated with the GENIE event generator code ([36], version 2.8.4). Both CC and NC interactions are simulated by GENIE. The event rates assume the neutrino fluxes described above, convoluted with the oscillation probabilities and the neutrino cross-sections. As a result, realistic estimates of ν_e, $\bar{\nu}_e$, ν_μ, $\bar{\nu}_\mu$, ν_τ, $\bar{\nu}_\tau$ interactions are obtained for each running mode.

Our assumptions for energy reconstruction capabilities of the DUNE far detector are discussed in section 2. Two scenarios are considered. First, the "CDR scenario" where

the energy smearing matrices for neutrino CC and NC interactions of the DUNE CDR are used [35]. The CC smearing matrices assume the energy-dependent resolutions shown in figures 4 for ν_e and ν_μ CC events. In the CDR scenario, 125 MeV wide bins in reconstructed neutrino energy are used. We have checked that essentially no gains are to be obtained by using finer energy bins in this case. Second, we consider a scenario with improved energy reconstruction capabilities, as motivated by this work. In this case, we parametrize the energy response of CC interactions with the gaussian resolution functions of eqs. (2.1)–(2.4). Furthermore, we use 50 MeV wide bins in reconstructed neutrino energy, to take full profit of the improved energy resolution assumptions. In the improved energy reconstruction scenario, we use the NC smearing matrices obtained from our LArSoft studies, see figure 5.

The strategy to extract oscillation parameters in DUNE is to perform a simultaneous fit to four far detector energy spectra: (1) ν_e or $\bar{\nu}_e$ CC candidate events in FHC running mode, (2) ν_e or $\bar{\nu}_e$ CC candidate events in RHC running mode, (3) ν_μ or $\bar{\nu}_\mu$ CC candidate events in FHC running mode, (4) ν_μ or $\bar{\nu}_\mu$ CC candidate events in RHC running mode. In our GLoBES description, we consider the same 32 oscillation channels as in the DUNE CDR, accounting for all signal and background components expected after selection cuts. We define 10 oscillation channels for the $\nu_\mu \to \nu_e$ appearance mode and 6 oscillation channels for the $\nu_\mu \to \nu_\mu$ disappearance mode, for both FHC and RHC running. The 32 oscillation channels are described in table 2 of [35].

Efficiencies to detect and reconstruct signal and background events are also taken from the DUNE CDR [20]. They are extracted using the DUNE Fast MC [43]. Efficiencies as a function of reconstructed neutrino energy for all 32 oscillation channels are provided in [35]. Compared to DUNE CDR assumptions, and only for our improved energy reconstruction scenario, we further select fiducial neutrino interactions with fully contained primary leptons (see section 2.1). We account for this by multiplying the DUNE CDR CC efficiencies by the efficiencies for primary lepton containment shown in figure 1.

Finally, and in addition to statistical uncertainties, we also consider the same signal and background normalization systematic uncertainties as in the DUNE CDR. We refer the reader to [20, 35] for details. The DUNE CDR treatment of systematic uncertainties is customized on a per-channel basis, and requires the use of GLoBES v3.2.16 or later.

3.2 Event rates and energy spectra

We conclude our description of the DUNE experimental setup by discussing the expected event rates in the DUNE far detector, for various event samples. We use GLoBES to extract the event rates. Each of the four far detector event samples is obtained under our two different detector performance assumptions, namely the CDR scenario and the improved energy reconstruction scenario. We summarize here the differences between the two descriptions:

1. Energy reconstruction for neutrino CC and NC interactions: our LArSoft-based studies (sections 2.1 and 2.3) versus DUNE CDR assumptions;

2. Oscillation analysis binning: 50 MeV versus 125 MeV wide bins in reconstructed neutrino energy;

Channel	Sample							
	ν_e CC		$\bar{\nu}_e$ CC		ν_μ CC		$\bar{\nu}_\mu$ CC	
$\overset{(-)}{\nu}_\mu \to \overset{(-)}{\nu}_e$ CC	**955.0**	(983.8)	**215.2**	(218.9)	0.0	(0.0)	0.0	(0.0)
$\overset{(-)}{\nu}_e \to \overset{(-)}{\nu}_e$ CC	203.6	(197.1)	104.9	(97.6)	0.0	(0.0)	0.0	(0.0)
$\overset{(-)}{\nu}_\mu \to \overset{(-)}{\nu}_\mu$ CC	2.8	(1.8)	1.6	(0.7)	**8439.8**	**(6546.9)**	**4164.0**	**(2978.8)**
$\overset{(-)}{\nu}_\mu \to \overset{(-)}{\nu}_\tau$ CC	18.7	(10.7)	10.8	(4.8)	29.2	(31.4)	18.2	(17.0)
$\overset{(-)}{\nu}$ NC	17.5	(20.0)	8.9	(8.3)	76.2	(47.3)	40.7	(21.4)

Table 2. Event rates for the four DUNE far detector samples, categorized in terms of oscillation channels. Bold-face numbers indicate signal events. The ν_e CC and ν_μ CC samples refer to events in FHC running mode passing the appearance and disappearance selection cuts, respectively. An exposure of 150 MW·kt·yr, NH and $\delta_{CP} = 0$ are assumed. The $\bar{\nu}_e$ CC and $\bar{\nu}_\mu$ labels indicate the corresponding RHC running mode samples, with the same assumptions. Events in the 0.5–8 GeV and 0.5–20 GeV energy ranges are considered for the $\overset{(-)}{\nu}_e$ and $\overset{(-)}{\nu}_\mu$ samples, respectively. Numbers outside parentheses are for the CDR scenario, numbers inside parentheses are for the improved energy reconstruction scenario.

3. Selection efficiency for ν_μ and $\bar{\nu}_\mu$ CC interactions: additional primary muon full containment requirement, versus no additional requirement compared to CDR efficiencies.

Unless otherwise noted, the following values for the oscillation parameters from Nu-Fit [6] are assumed: $\Delta m^2_{21} = (7.50 \pm 0.19) \cdot 10^{-5}$ eV^2, $\Delta m^2_{31} = (2.457 \pm 0.047) \cdot 10^{-3}$ eV^2, $\theta_{12} = 33.48° \pm 0.78°$, $\theta_{13} = 8.50°$ and $\theta_{23} = 42.3°$. The final results, unless stated, are marginalized over all other oscillation parameters within their allowed priors. In the case of θ_{13} and θ_{23} the gaussian prior representing our current constraints on these parameters are rather included for $\sin^2 2\theta$, which is a more accurate description of the present situation and, in the case of θ_{23}, allows to properly account for the octant degeneracy. Again following Nu-Fit [6] we take 0.005 and 0.02 as the present errors on $\sin^2 2\theta_{13}$ and $\sin^2 2\theta_{23}$ respectively. Finally, a 2% uncertainty in the PREM density profile assumed has also been considered. In general, results will either be presented as a function of the less known parameters δ_{CP}, θ_{23} and the mass hierarchy or as bands whose width is determined by varying these parameters in their currently allowed range.

Table 2 shows the event rates integrated over neutrino energy, for the various samples and for the two experimental descriptions considered. For an exposure of 150 MW·kt·yr in FHC running mode, approximately 10^3 $\nu_e + \bar{\nu}_e$ CC candidates are expected at the far detector, together with about 10^4 $\nu_\mu + \bar{\nu}_\mu$ CC candidates. For the same exposure, the event statistics is significantly lower in RHC running mode. For the CDR scenario, the signal and background rates in table 2 match those given in [20]. For the improved energy reconstruction scenario, lower $\nu_\mu + \bar{\nu}_\mu$ CC rates are expected because of the additional full muon containment requirement. As table 2 shows, this efficiency loss is relatively mild, at the 20–30% level, for events in the entire 0.5–20 GeV energy range, and even lower in the low-energy portion (0.5–6 GeV) that is most relevant for neutrino oscillation measurements.

The expected $\nu_e + \bar{\nu}_e$ CC candidate events in FHC running mode and as a function of reconstructed neutrino energy are shown in the upper panels of figure 6, for the two
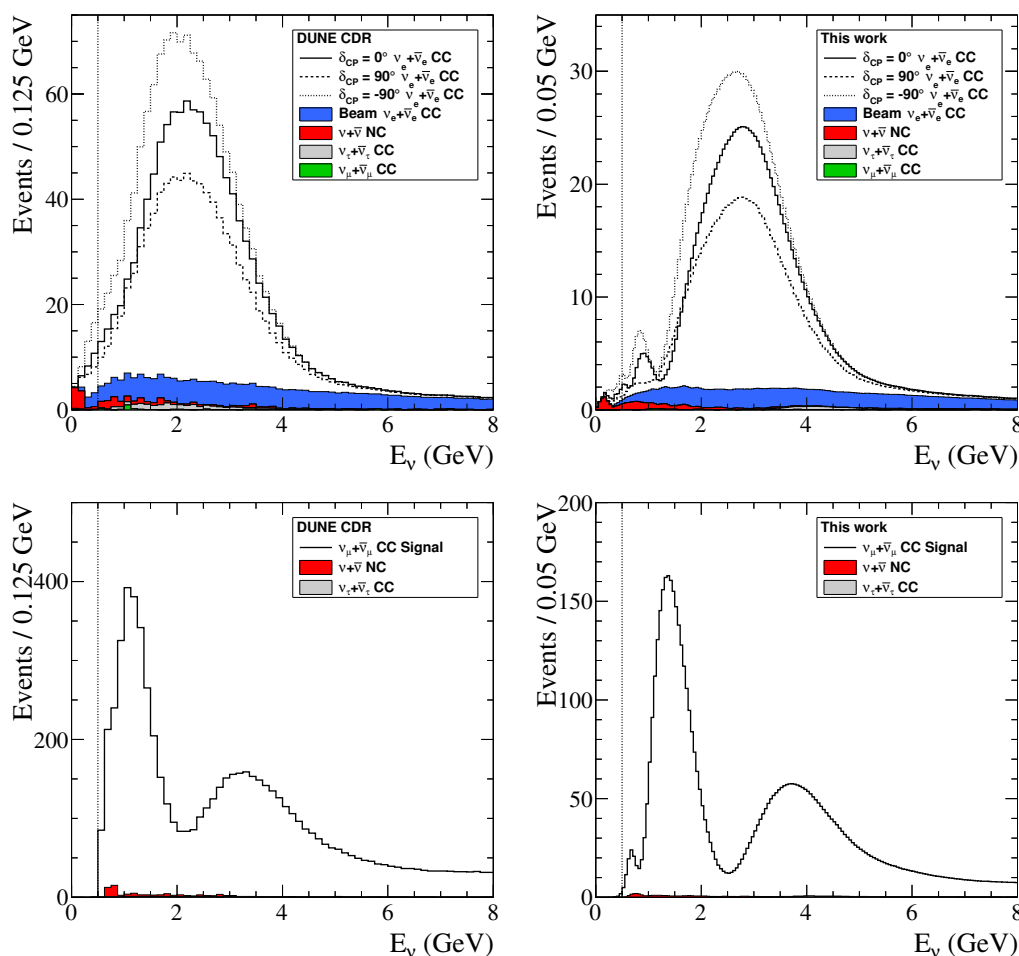
Figure 6. Expected number of $\nu_e + \bar{\nu}_e$ CC (upper panels) and $\nu_\mu + \bar{\nu}_\mu$ CC (lower panels) candidate events in FHC running mode and as a function of reconstructed neutrino energy. Background events are shown with filled histograms, signal events with lines. Three different ν_e signal scenarios are shown in the upper panels. The neutrino energy reconstruction capabilities of the DUNE CDR [20] are assumed in the left panels, while the reconstruction performance expected from this work are shown on the right ones. An exposure of 150 MW·kt·yr and NH are assumed.

scenarios described above, DUNE CDR (left) and our own assumptions (right). In the case of improved energy resolution and finer binning, a much improved determination of the second oscillation maximum at 0.8 GeV appears possible. A similar result is obtained by examining the expected $\nu_e + \bar{\nu}_e$ CC candidate events in RHC running mode.

The $\nu_\mu + \bar{\nu}_\mu$ CC candidate event predictions in FHC mode and as a function of energy are shown in the lower panels of figure 6. An improved determination of the first oscillation dip near 2.5 GeV, and even a hint for a second oscillation dip around 0.8 GeV, appear possible with the improved reconstruction and finer analysis binning case shown in the right panel. As noted above, the efficiency loss for full muon containment has a small effect on the event rates across the relevant energy range. Again, similar conclusions are obtained for RHC mode spectra.

In the rest of this paper, we address how these improvements in spectral information translate in improvements in long-baseline oscillation sensitivities.

– 13 –

4 Results

The search for the remaining unknown neutrino oscillation parameters, in particular for the CP-violating phase $\delta_{\rm CP}$, requires the study of genuinely three-flavor oscillation effects through the so-called "golden channel" $\nu_{\mu,e} \to \nu_{e,\mu}$. Neglecting higher-order terms in $\alpha \equiv |\Delta m^2_{21}|/|\Delta m^2_{31}| \sim 0.03$ and in $\sin\theta_{13} \sim 0.15$, the oscillation probability[1] of $\nu_\mu \to \nu_e$ for DUNE can be cast as [48, 49]:

$$
\begin{aligned}
P(\nu_\mu \to \nu_e) \cong\ & \sin^2\theta_{23} \sin^2 2\theta_{13} \frac{\sin^2[\Delta(A-1)]}{(A-1)^2} \\
& + \alpha J \sin\delta_{\rm CP} \sin\Delta \frac{\sin(A\Delta)\sin[(1-A)\Delta]}{A(1-A)} \\
& + \alpha J \cos\delta_{\rm CP} \cos\Delta \frac{\sin(A\Delta)\sin[(1-A)\Delta]}{A(1-A)} \\
& + \alpha^2 \cos^2\theta_{23} \sin^2 2\theta_{12} \cos^2\theta_{13} \frac{\sin^2(A\Delta)}{A^2},
\end{aligned}
\tag{4.1}
$$

where $J = \cos\theta_{13} \sin 2\theta_{13} \sin 2\theta_{12} \sin 2\theta_{23}$, $\Delta = \Delta m^2_{31} L/4E$, $A = 2\sqrt{3} G_F n_e E/\Delta m^2_{31}$, G_F is the weak coupling constant and n_e is the number density of electrons in the propagation medium. An asymmetry in neutrino versus antineutrino oscillations is induced both by the presence of a CP-odd term ($\propto \sin\delta_{\rm CP}$) and by the matter effect A, which changes sign going from $\nu_\mu \to \nu_e$ to the $\bar\nu_\mu \to \bar\nu_e$ channel. The asymmetry induced by the matter effect depends on the sign of Δm^2_{31} and increases with the neutrino energy (E) and the baseline (L). The degeneracy between the CP-violation and matter effect induced asymmetries can thus be resolved with long baselines and high energies, like the ones adopted by DUNE. This experiment enhances so much the matter effect that the associated asymmetry cannot be mimicked by any possible value of $\delta_{\rm CP}$. In this case the CP-violating asymmetry would represent a far more sub-leading — and therefore challenging to discover — effect.

On the other hand, these strong matter effects not only lead to a great enhancement of the (anti)neutrino channel for NH (IH), but also to the suppression of the oscillation probability for the other channel. This implies that the search for leptonic CP violation cannot rely so strongly on its most natural physics effect: an asymmetry between the neutrino and antineutrino oscillation probabilities — since one of them is very suppressed; it must rather exploit the characteristic energy dependence of the CP-violating term in eq. (4.1).

Furthermore, the fact that θ_{13} turned out to be relatively large, saturating previous upper bounds, implies that the expansion in eq. (4.1) is not symmetric since the terms suppressed by $\sin\theta_{13} \sim 0.15$ dominate over those suppressed by $\alpha \sim 0.03$. In particular, the first term of the equation tends to dominate over the second and third, which are those containing the dependence on $\delta_{\rm CP}$. A possible way to alleviate this is to observe the oscillation probability beyond the first oscillation peak, so that the slower, Δm^2_{21}-driven oscillation has developed further and the CP-violating interference with the $\sin\theta_{13}$-modulated term represents a more significant contribution to the final oscillation probability [50–52]. Thus, one of the widely-advertised benefits of a wide-band beam — such as the one envisioned for

---

[1]This approximation will only be used to interpret the results presented in this section, while all the numerical results have been computed with the exact matter oscillation probability.

the DUNE experiment — is that it would allow to cover not only the first oscillation peak, but also beyond it and, in particular, the second oscillation maximum. However, in ref. [53] it was shown that for a wide-band beam, the significantly lower statistics present at the second oscillation peak due to the smaller flux (typically at the tail) and cross section (at lower energies), combined with the large background from NC interactions migrating from higher energies, rendered the information coming from the second peak nearly irrelevant (see also [54]).[2] Thus, an improved energy reconstruction can be beneficial to the search for leptonic CP violation in two ways. On the one hand it helps with the measurement of $\delta_{\rm CP}$ through the characteristic energy dependence of the second and third terms in eq. (4.1). On the other hand, it can enhance the relevance of the measurements at the second oscillation peak as shown in figure 6, particularly when combined with the optimized beam design recently adopted, which peaks at lower energies.

In the rest of this section we will present sensitivity studies for: (1) the MH, (2) $\delta_{\rm CP}$ and (3) θ_{23}. All experimental sensitivities are estimated using the GLoBES package [44], and are obtained for the DUNE experiment description and for the priors in the neutrino oscillation parameters described in section 3.

4.1 Sensitivity to mass hierarchy

The neutrino mass hierarchy, that is the sign of Δm^2_{31}, controls the sign of the matter potential A in eq. (4.1) and it can thus lead to an enhancement (suppression) of the neutrino oscillation probability for normal (inverted) hierarchy, with an opposite effect for antineutrino oscillations. This effect is already present (and quadratic) in the first term of eq. (4.1) which, given that $\sin\theta_{13} > \alpha$, turns out to dominate the oscillation probability. Thus, for the long-baseline and high neutrino energies that characterize the DUNE setup, large matter effects, and hence very good sensitivity to the neutrino mass hierarchy, are expected.

We quantify the MH discovery potential through the χ^2 difference between the two hierarchies:

$$\Delta\chi^2_{\rm MH} = \chi^2_{\rm IH} - \chi^2_{\rm NH}, \text{ (for true normal hierarchy)}$$
$$\Delta\chi^2_{\rm MH} = \chi^2_{\rm NH} - \chi^2_{\rm IH}, \text{ (for true inverted hierarchy)}. \tag{4.2}$$

Notice that some deviations from a χ^2 distribution are expected for this observable, however, these have been quantitatively evaluated to be small [58].

The sensitivity of DUNE to the MH determination depends on the actual values of $\delta_{\rm CP}$ and θ_{23}, apart from the true value of the MH itself. On the one hand, the role of $\delta_{\rm CP}$ is similar to that of the MH since it induces an asymmetry in the neutrino vs antineutrino oscillation probabilities. Indeed, NH and $\delta_{\rm CP} \sim -\pi/2$ will both enhance (suppress) the (anti)neutrino oscillations, while an IH and $\delta_{\rm CP} \sim \pi/2$ would have the opposite effect. Thus, any of these two combinations would lead to the best sensitivities to both the MH and the CP-violating phase, while cases with NH and $\delta_{\rm CP} \sim \pi/2$ or IH and $\delta_{\rm CP} \sim -\pi/2$ tend to compensate each other leading to an altogether weaker effect and lower sensitivities. Regarding θ_{23}, since the sensitivity to the MH mainly stems from the first term in eq. (4.1),

---

[2]An interesting alternative for experiments with high statistics is to center the beam energy at the second oscillation peak, which can significantly increase the sensitivity to $\delta_{\rm CP}$ [55–57].
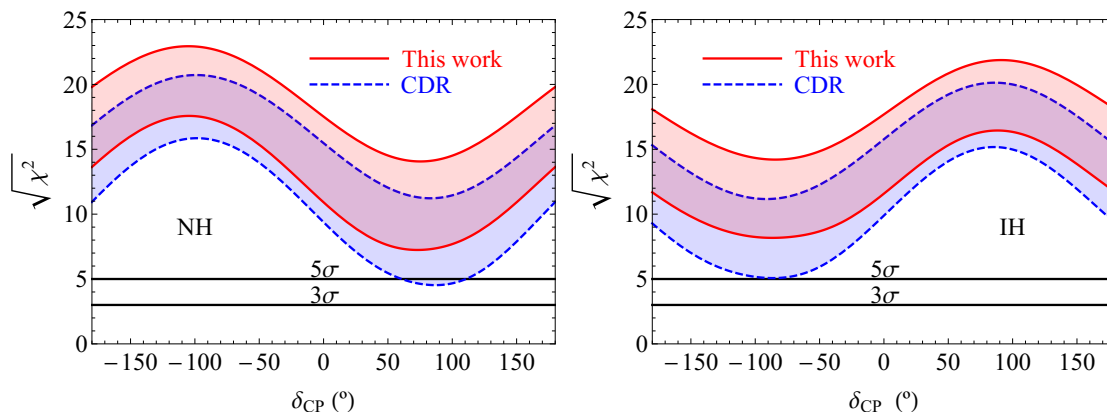
Figure 7. Mass hierarchy discovery potential for DUNE at a fiducial exposure of 1.07 MW ×40 kton×7 yr. The plot on the left is for NH, the one on the right is for IH. Blue, dashed curves refer to the significance with which the MH can be determined, as a function of δ_{CP}, for the DUNE CDR setup. Red, solid curves show the expected sensitivity for the improved energy reconstruction discussed in this work. The width of the band corresponds to letting the assumed true value of θ_{23} vary from $\theta_{23} = 38°$ (lower sensitivity) to $\theta_{23} = 53°$ (higher sensitivity) as allowed by current global fits.

proportional to $\sin^2 \theta_{23}$, larger values of θ_{23} are preferred to enhance the effect and increase the sensitivity. For these reasons, we perform a scan over all possible values of δ_{CP}^{true} and show the results for a range of true values of θ_{23} allowed by current global fits [6, 59, 60].

Figure 7 shows the significance (under the assumption of a χ^2 distribution) with which the MH could be determined as a function of the value of δ_{CP}^{true}, for an exposure of $3.5 + 3.5$ years (in FHC and RHC modes, respectively), with a 40 kt detector and a 1.07 MW beam. With this exposure, the MH may be determined with a minimum significance of $\sqrt{\Delta\chi^2_{MH}} = 5$ for any δ_{CP} value for the DUNE CDR detector performance scenario (blue dashed curves) except for NH close to $\delta_{CP} \sim \pi/2$ and for small θ_{23} where the significance is slightly over 4σ. This sensitivity is enhanced by at least 2σ for the improved energy reconstruction scenario motivated by this paper (red solid curves). Even the least favorable combination of $(\theta_{23}, \delta_{CP}, MH)$ parameters would allow to disentangle the MH with a significance of $\sim 7\sigma$ in the improved reconstruction scenario.

4.2 Sensitivity to CP violation and precision in δ_{CP}

DUNE aims at the observation of leptonic CP violation (CPV). Within the standard framework of three neutrino flavours, such a signal will be observable if the value of the CP violating phase is sufficiently different from 0 or π, cases in which there is no CP violation. Furthermore, the sensitivity to δ_{CP} stems solely from the second and third terms in eq. (4.1). Therefore, smaller values of θ_{23}, which suppress the dominant first term in the equation, tend to increase the sensitivity to leptonic CP violation. We infer the CP violation discovery potential of DUNE at a given value δ_{CP}^{true} by minimising the $\Delta\chi^2$:

$$\Delta\chi^2_{CPV} = \min\left[\Delta\chi^2_{CP}(\delta_{CP}^{test} = 0), \Delta\chi^2_{CP}(\delta_{CP}^{test} = \pi)\right], \text{ where} \tag{4.3}$$

$$\Delta\chi^2_{CP} = \chi^2_{\delta_{CP}^{test}} - \chi^2_{\delta_{CP}^{true}}. \tag{4.4}$$
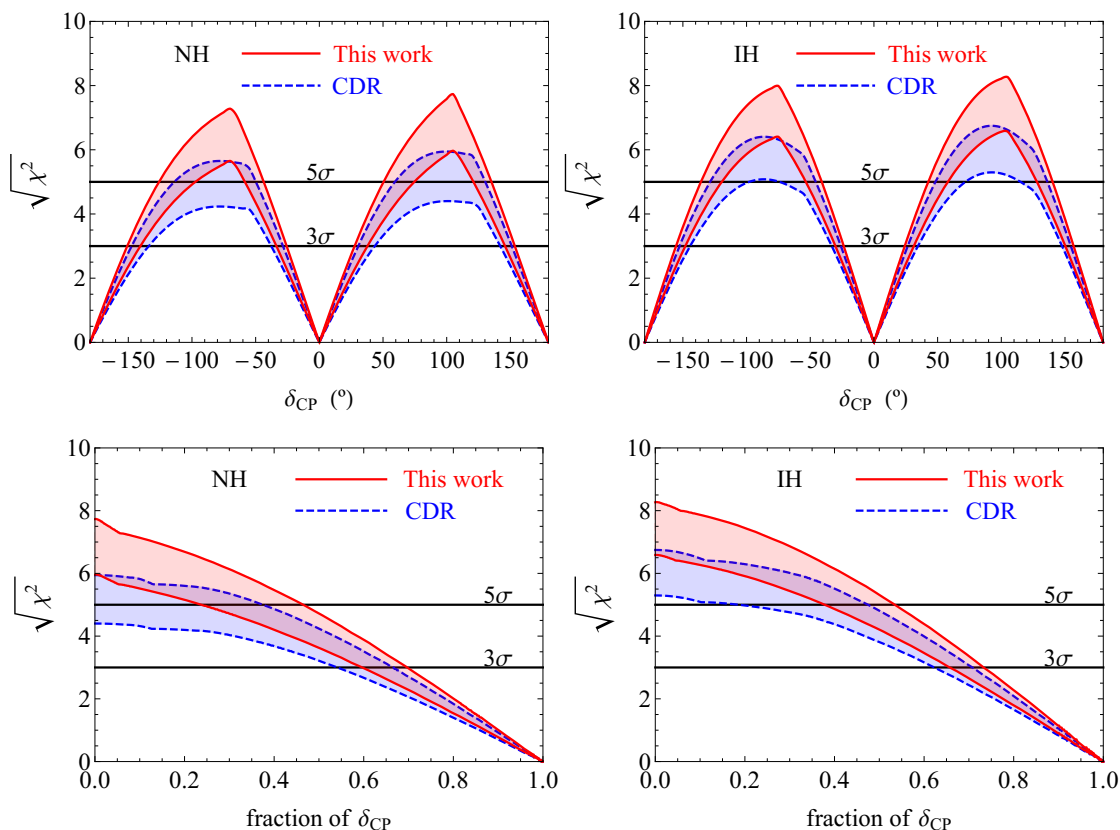
Figure 8. CP violation discovery potential ($\delta_{\rm CP} \neq 0, \pi$) at DUNE, assuming a fiducial exposure of 1.07 MW$\times$40 kton$\times$7 yr, as a function of $\delta_{\rm CP}$. The plot on the left is for NH, the one on the right is for IH. Blue, dashed curves refer to the DUNE CDR setup. Red, solid curves show the expected discovery potential for the improved energy reconstruction discussed in this work. The width of the band corresponds to letting the assumed true value of θ_{23} vary from $\theta_{23} = 53°$ (lower sensitivity) to $\theta_{23} = 38°$ (higher sensitivity) as allowed by current global fits. The lower panels convey the same information, but as a function of the fraction of values of $\delta_{\rm CP}$ for which a given significance could be achieved.

Even though the cyclic nature of $\delta_{\rm CP}$ has been shown to induce important deviations from a χ^2 distribution, these are mainly relevant for present facilities [61–63] and their impact for the DUNE setup should be mild.

Sensitivities as a function of $\delta_{\rm CP}^{\rm true}$ are shown in figure 8 for a range of true values of θ_{23} allowed by current global fits, for both NH and IH. Solid black lines corresponding to 3σ and 5σ significance, which indicate 99.73% and 99.99% probability respectively, of determining CP-violation (under a χ^2 distribution assumption) are also shown for comparison. We also show in the lower panels the same information, but as a function of the fraction of values of $\delta_{\rm CP}$ that would allow a discovery of CPV at the corresponding significance.

For the DUNE CDR scenario, a 3σ evidence for CPV could be achieved for $\sim 60\%$ ($\sim 65\%$) of the possible values of $\delta_{\rm CP}$ for NH (IH), depending on the actual value of θ_{23}. These values would increase by $\sim 5\%$ with the improved energy reconstruction discussed here. The improvement is however more dramatic for the 5σ discovery mark. In this case, under the CDR assumptions, a maximum of 37% (47%) of the possible values of $\delta_{\rm CP}$ for
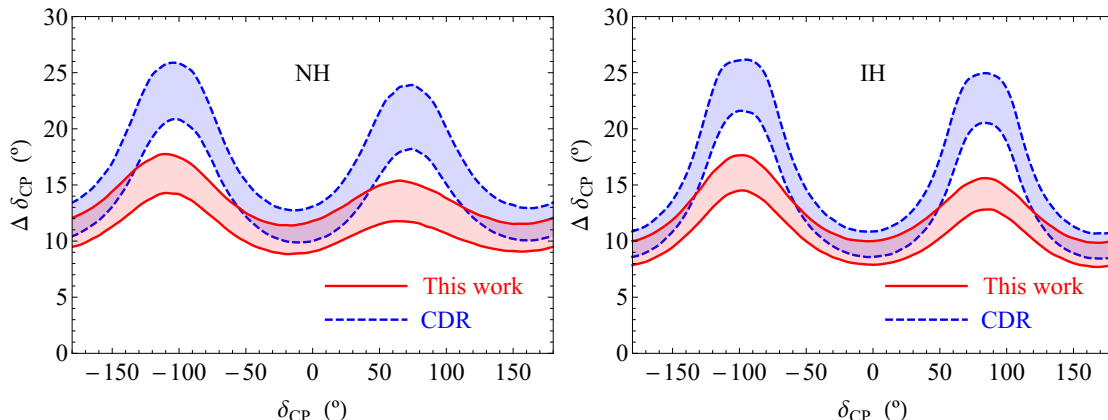
Figure 9. Half-size of the allowed 1σ region to which δ_{CP} would be constrained at DUNE, assuming a fiducial exposure of 1.07 MW×40 kton×7 yr, as a function of δ_{CP}. The plot on the left is for NH, the one on the right is for IH. Blue, dashed curves refer to the DUNE CDR setup. Red, solid curves show the expected discovery potential for the improved energy reconstruction discussed in this work. The width of the band corresponds to letting the assumed true value of θ_{23} vary from $\theta_{23} = 53°$ (smaller error) to $\theta_{23} = 38°$ (larger error) as allowed by current global fits.

NH (IH) would be covered for favorable values of θ_{23}, while no values of δ_{CP} would allow for such a discovery for the least favorable θ_{23} values. With improved energy reconstruction, these numbers are improved to 47% (53%), and a minimum 24% coverage is obtained even for the least favorable θ_{23} values.

In figure 9 we show the δ_{CP} uncertainties, defined as the half-size of the 1σ region to which δ_{CP} would be constrained at DUNE. For the CDR setup (blue dashed curves) this error would range between 9° and 26°. The smallest uncertainties correspond to small values of θ_{23} (minimizing the competing CP-conserving term in eq. (4.1)) and to nearly CP-conserving δ_{CP} values, although slightly shifted to the left due to matter effects (see ref. [64] for a detailed explanation of this effect). The improved energy reconstruction greatly reduces the δ_{CP} uncertainties around the maximally CP-violating values of δ_{CP}, translating into a δ_{CP} precision ranging between 8° and 18°. This very pronounced improvement for CP-violating values of δ_{CP} is also apparent in the substantial gain in the 5σ coverage of the CP-violation discovery potential shown in figure 8. We have verified that these gains stem significantly from the improved observation of the second oscillation maximum thanks to the better energy resolution. Indeed, when restricting the analysis to the higher energy bins so that the second maximum in not analyzed, the improvement between the CDR scenario and the one with better energy reconstruction is notably milder. As noted above, we have also verified that the finer (50 MeV compared to 125 MeV) energy binning has no impact on the sensitivities if combined with the CDR energy reconstruction. In other words, the effect is entirely caused by the improved energy reconstruction.

4.3 Sensitivity to θ_{23} octant degeneracy and to deviations from maximal mixing

Current global fit analyses [6, 59, 60] find good agreement with experimental data for values of θ_{23} slightly above and below $\pi/4$. This stems from the fact that, at present,
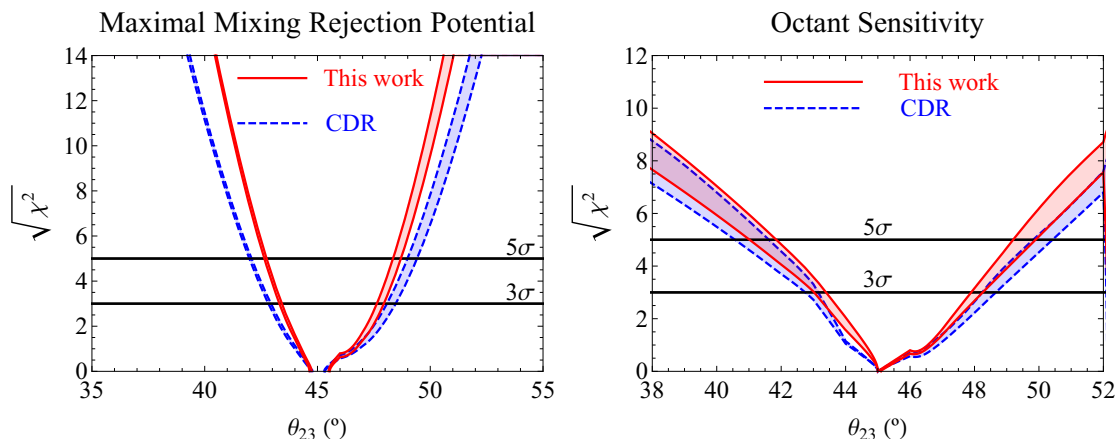
Figure 10. Maximal mixing rejection potential (left) and octant discovery potential (right) of DUNE, assuming a fiducial exposure of 1.07 MW×40 kton×7 yr. Blue, dashed curves refer to the DUNE CDR setup. Red, solid curves show the expected discovery potential for the improved energy reconstruction discussed in this work. The width of the band corresponds to allowing δ_{CP} to vary in its whole range as well as allowing both possible mass hierarchies.

the measurements of this parameter are dominated by the ν_μ disappearance channel, with a leading dependence on $\sin 2\theta_{23}$, which induces this degeneracy. Furthermore, maximal mixing is only mildly disfavored in these fits and remains a perfectly viable possibility. It is thus interesting to explore the sensitivity of DUNE to rule out maximal mixing and to determine its correct octant (if θ_{23} turns out not to be maximal). This information is particularly interesting for models aiming at explaining the observed pattern of neutrino masses and mixings through symmetry arguments, since deviations of θ_{23} from maximal mixing tend to be correlated with the value of θ_{13} or even δ_{CP}.

With DUNE, the maximal mixing and the octant hypotheses can be probed via a synergistic measurement of both $\nu_\mu \to \nu_\mu$ and $\nu_\mu \to \nu_e$ oscillations, sensitive to $\sin^2 2\theta_{23}$ and to $\sin^2 \theta_{23}$, respectively. We define the $\Delta\chi^2$ metric in the two cases as:

$$\Delta\chi^2_{\mathrm{maxmix}} = \chi^2(\theta_{23} = 45°) - \chi^2(\theta_{23}^{\mathrm{true}}),$$
$$\Delta\chi^2_{\mathrm{octant}} = \chi^2(\pi/2 - \theta_{23}^{\mathrm{true}}) - \chi^2(\theta_{23}^{\mathrm{true}}). \tag{4.5}$$

In this analysis we do not impose the gaussian prior on $\sin^2 2\theta_{23}$.

The left panel of figure 10 shows the maximal mixing rejection potential, that is, the significance (assuming a χ^2 distribution) with which the maximal mixing hypothesis would be disfavored as a function of the true value of θ_{23}. Values as close to 45° as 42° (43°) or 50° (49°) for the CDR (improved energy reconstruction) setup could be distinguished from maximal mixing at 5σ significance. For comparison, the 5σ range in θ_{23} from global fits to existing neutrino oscillation data lies in the range 36°–56° [6]. In the right panel of figure 10 the significance (under the assumption of a χ^2 distribution) with which the octant degeneracy could be solved is shown. For the CDR (improved energy reconstruction) setup a discovery of the octant would be guaranteed, unless θ_{23} lies in in the interval 40° − 51° (41° − 50°). For these two measurements the sensitivity mainly stems from the combination of the appearance and disappearance channels. Therefore, the better resolution of the second oscillation maximum and the improved energy reconstruction are less relevant, and

– 19 –

translate in a less significant gain compared to the δ_{CP} measurement. In this case, the lower statistics in the disappearance channel for the improved energy reconstruction setup, due to the additional requirement of full muon containment, also plays a role.

5 Conclusions

In this work we have explored the gains in DUNE long-baseline neutrino oscillation sensitivities that can be obtained with improved neutrino energy reconstruction capabilities, compared to what is customarily assumed.

The neutrino energy reconstruction performance for neutrino charged-current interactions of all relevant flavors and energies has been evaluated via detailed simulations of a DUNE liquid argon far detector module. Our simulations account for nuclear effects in neutrino-argon interactions, energy leakage out of the detector active volume, ionization quenching, and electron-ion recombination, while we neglect drift and readout effects. Our studies indicate that an energy reconstruction performance significantly better than what was assumed in the DUNE Conceptual Design Report (CDR, [20]) is in principle possible, particularly at low neutrino energies.

We find that this improved energy reconstruction not only allows DUNE to better resolve the characteristic energy dependence of the CP-violating term. It can also allow the experiment to reconstruct much more clearly the second oscillation maximum of the $\nu_\mu \to \nu_e$ oscillation, particularly sensitive to the unknown CP-violating phase δ_{CP}. In combination with DUNE's optimized neutrino beamline design, yielding a larger flux at low energies compared to the previous reference design, the improved energy reconstruction translates into a significant increase in the physics reach of the DUNE search for δ_{CP}. Indeed, for an exposure of of $3.5 + 3.5$ years (in forward horn current and reverse horn current modes, respectively), with a 40 kt fiducial mass detector and a 1.07 MW beam, the improved energy reconstruction translates into an increase of the fraction of δ_{CP} values allowing for a 5σ discovery of leptonic CP violation from 0 % (47 %) to 24 % (53 %) for the least (most) favorable combination of the other neutrino oscillation parameters allowed by current data. The precision of a δ_{CP} measurement would also increase significantly, from a maximum uncertainty of $26°$ with standard (DUNE CDR) detector response, to $18°$ with improved energy reconstruction. The significance of the mass hierarchy determination would also increase by at least two standard deviations for any value of δ_{CP}.

Conversely, the precision measurements of θ_{23} do not benefit as much from the improved energy reconstruction, relying more in the comparison of appearance and disappearance channels than in the coverage of the second oscillation maximum. Still, a modest increase of $\sim 2°$ in the range of θ_{23} values that would allow for either a 5σ determination of the octant or for a rejection of maximal mixing, would be achieved.

We expect that the benefits to the DUNE oscillation sensitivities from improved energy reconstruction could be somewhat reduced by the inclusion of energy shape systematic uncertainties. Energy shape-only systematic uncertainties have been neglected both in the DUNE CDR and in our own studies. Future analyses, adopting a more comprehensive systematic uncertainty treatment, will therefore prove to be interesting. In any case, we conclude that the observed gain in DUNE physics reach is strong enough to justify further exploration of the energy reconstruction capabilities ultimately achievable with large liquid argon neutrino detectors, and particularly with DUNE.

Acknowledgments

References

[1] B. Pontecorvo, *Mesonium and anti-mesonium*, *Sov. Phys. JETP* **6** (1957) 429 [*Zh. Eksp. Teor. Fiz.* **33** (1957) 549].

[2] B. Pontecorvo, *Inverse beta processes and nonconservation of lepton charge*, *Sov. Phys. JETP* **7** (1958) 172 [*Zh. Eksp. Teor. Fiz.* **34** (1957) 247].

[3] Z. Maki, M. Nakagawa, Y. Ohnuki and S. Sakata, *A unified model for elementary particles*, *Prog. Theor. Phys.* **23** (1960) 1174 [INSPIRE].

[4] Z. Maki, M. Nakagawa and S. Sakata, *Remarks on the unified model of elementary particles*, *Prog. Theor. Phys.* **28** (1962) 870 [INSPIRE].

[5] B. Pontecorvo, *Neutrino experiments and the problem of conservation of leptonic charge*, *Sov. Phys. JETP* **26** (1968) 984 [INSPIRE].

[6] M.C. Gonzalez-Garcia, M. Maltoni and T. Schwetz, *Updated fit to three neutrino mixing: status of leptonic CP-violation*, *JHEP* **11** (2014) 052 [arXiv:1409.5439] [INSPIRE].

[7] DAYA BAY collaboration, F.P. An et al., *Observation of electron-antineutrino disappearance at Daya Bay*, *Phys. Rev. Lett.* **108** (2012) 171803 [arXiv:1203.1669] [INSPIRE].

[8] RENO collaboration, J.K. Ahn et al., *Observation of reactor electron antineutrino disappearance in the RENO experiment*, *Phys. Rev. Lett.* **108** (2012) 191802 [arXiv:1204.0626] [INSPIRE].

[9] DOUBLE CHOOZ collaboration, Y. Abe et al., *Reactor electron antineutrino disappearance in the Double CHOOZ experiment*, *Phys. Rev.* **D 86** (2012) 052008 [arXiv:1207.6632] [INSPIRE].

[10] MINOS collaboration, P. Adamson et al., *Improved search for muon-neutrino to electron-neutrino oscillations in MINOS*, *Phys. Rev. Lett.* **107** (2011) 181802 [arXiv:1108.0015] [INSPIRE].

[11] T2K collaboration, K. Abe et al., *Indication of electron neutrino appearance from an accelerator-produced off-axis muon neutrino beam*, *Phys. Rev. Lett.* **107** (2011) 041801 [arXiv:1106.2822] [INSPIRE].

[12] PARTICLE DATA GROUP collaboration, K.A. Olive et al., *Review of particle physics*, *Chin. Phys.* **C 38** (2014) 090001 [INSPIRE].

[13] M.B. Gavela, P. Hernández, J. Orloff and O. Pene, *Standard model CP-violation and baryon asymmetry*, *Mod. Phys. Lett.* **A 9** (1994) 795 [hep-ph/9312215] [INSPIRE].

[14] M.B. Gavela, P. Hernández, J. Orloff, O. Pene and C. Quimbay, *Standard model CP-violation and baryon asymmetry. Part 2: finite temperature*, *Nucl. Phys.* **B 430** (1994) 382 [hep-ph/9406289] [INSPIRE].

[15] T2K collaboration, K. Abe et al., *Observation of electron neutrino appearance in a muon neutrino beam*, *Phys. Rev. Lett.* **112** (2014) 061802 [arXiv:1311.4750] [INSPIRE].

[16] NOvA collaboration, P. Adamson et al., *First measurement of electron neutrino appearance in NOvA*, *Phys. Rev. Lett.* **116** (2016) 151806 [arXiv:1601.05022] [INSPIRE].

[17] F. Capozzi, E. Lisi, A. Marrone, D. Montanino and A. Palazzo, *Neutrino masses and mixings: status of known and unknown 3ν parameters*, *Nucl. Phys.* **B 908** (2016) 218 [arXiv:1601.07777] [INSPIRE].

[18] M. Gonzalez-Garcia, M. Maltoni, and T. Schwetz, *NuFIT 2.1*, http://www.nu-fit.org (2016).

[19] M. Fukugita and T. Yanagida, *Baryogenesis without grand unification*, *Phys. Lett.* **B 174** (1986) 45 [INSPIRE].

[20] DUNE collaboration, R. Acciarri et al., *Long-Baseline Neutrino Facility (LBNF) and Deep Underground Neutrino Experiment (DUNE)*, arXiv:1512.06148 [INSPIRE].

[21] M. Sorel, *Expected performance of an ideal liquid argon neutrino detector with enhanced sensitivity to scintillation light*, 2014 *JINST* **9** P10002 [arXiv:1405.0848] [INSPIRE].

[22] A.M. Ankowski et al., *Comparison of the calorimetric and kinematic methods of neutrino energy reconstruction in disappearance experiments*, *Phys. Rev.* **D 92** (2015) 073014 [arXiv:1507.08560] [INSPIRE].

[23] MINOS collaboration, D.G. Michael et al., *The magnetized steel and scintillator calorimeters of the MINOS experiment*, *Nucl. Instrum. Meth.* **A 596** (2008) 190 [arXiv:0805.3170] [INSPIRE].

[24] NOvA collaboration, P. Adamson et al., *First measurement of muon-neutrino disappearance in NOvA*, *Phys. Rev.* **D 93** (2016) 051104 [arXiv:1601.05037] [INSPIRE].

[25] A. Ferrari and P.R. Sala, *Physics processes in hadronic showers*, *Frascati Phys. Ser.* **21** (2001) 31.

[26] C. Rubbia et al., *Underground operation of the ICARUS T600 LAr-TPC: first results*, 2011 *JINST* **6** P07011 [arXiv:1106.0975] [INSPIRE].

[27] A. Stahl et al., *Expression of interest for a very Long Baseline Neutrino Oscillation experiment (LBNO)*, CERN-SPSC-2012-021 (2012).

[28] A.M. Ankowski, P. Coloma, P. Huber, C. Mariani and E. Vagnoni, *Missing energy and the measurement of the CP-violating phase in neutrino oscillations*, *Phys. Rev.* **D 92** (2015) 091301 [arXiv:1507.08561] [INSPIRE].

[29] LArIAT collaboration, F. Cavanna, M. Kordosky, J. Raaf and B. Rebel, *LArIAT: Liquid Argon In A Testbeam*, arXiv:1406.5560 [INSPIRE].

[30] L. Agostino et al., *LBNO-DEMO: large-scale neutrino detector demonstrators for phased performance assessment in view of a long-baseline oscillation experiment*, arXiv:1409.4405 [INSPIRE].

[31] T. Kutter, *Proposal for a full-scale prototype single-phase liquid argon time projection chamber and detector beam test at CERN*, CERN-SPSC-2015-020 (2015).

[32] CAPTAIN collaboration, H. Berns et al., *The CAPTAIN detector and physics program*, arXiv:1309.1740 [INSPIRE].

[33] ICARUS collaboration, A. Ankowski et al., *Energy reconstruction of electromagnetic showers from pi0 decays with the ICARUS T600 Liquid Argon TPC*, *Acta Phys. Polon.* **B 41** (2010) 103 [arXiv:0812.2373] [INSPIRE].

[34] E.D. Church, *LArSoft: A Software Package for Liquid Argon Time Projection Drift Chambers*, arXiv:1311.6774 [INSPIRE].

[35] DUNE collaboration, T. Alion et al., *Experiment simulation configurations used in DUNE CDR*, arXiv:1606.09550 [INSPIRE].

[36] C. Andreopoulos et al., *The GENIE neutrino Monte Carlo generator*, *Nucl. Instrum. Meth.* **A 614** (2010) 87 [arXiv:0905.2517] [INSPIRE].

[37] GEANT4 collaboration, S. Agostinelli et al., *GEANT4: a simulation toolkit*, *Nucl. Instrum. Meth.* **A 506** (2003) 250 [INSPIRE].

[38] GEANT4 HADRONIC GROUP collaboration, J. Yarba, *Recent developments and validation of Geant4 hadronic physics*, *J. Phys. Conf. Ser.* **396** (2012) 022060 [INSPIRE].

[39] M. Szydagis et al., *NEST: a comprehensive model for scintillation yield in liquid xenon*, 2011 *JINST* **6** P10002 [arXiv:1106.1613] [INSPIRE].

[40] T. Doke et al., *Let dependence of scintillation yields in liquid argon*, *Nucl. Instrum. Meth.* **A 269** (1988) 291 [INSPIRE].

[41] M. Miyajima et al., *Average energy expended per ion pair in liquid argon*, *Phys. Rev.* **A 9** (1974) 1438 [INSPIRE].

[42] DUNE collaboration, R. Acciarri et al., *Long-Baseline Neutrino Facility (LBNF) and Deep Underground Neutrino Experiment (DUNE)*, arXiv:1601.02984 [INSPIRE].

[43] LBNE collaboration, C. Adams et al., *The Long-Baseline Neutrino Experiment: exploring fundamental symmetries of the Universe*, arXiv:1307.7335 [INSPIRE].

[44] P. Huber, M. Lindner and W. Winter, *Simulation of long-baseline neutrino oscillation experiments with GLoBES (General Long Baseline Experiment Simulator)*, *Comput. Phys. Commun.* **167** (2005) 195 [hep-ph/0407333] [INSPIRE].

[45] P. Huber, J. Kopp, M. Lindner, M. Rolinec and W. Winter, *New features in the simulation of neutrino oscillation experiments with GLoBES 3.0: general long baseline experiment simulator*, *Comput. Phys. Commun.* **177** (2007) 432 [hep-ph/0701187] [INSPIRE].

[46] A.M. Dziewonski and D.L. Anderson, *Preliminary reference Earth model*, *Phys. Earth Planet. Interiors* **25** (1981) 297.

[47] F. Stacey, *Physics of the Earth*, 2nd edition, Wiley, U.S.A. (1977).

[48] A. Cervera et al., *Golden measurements at a neutrino factory*, *Nucl. Phys.* **B 579** (2000) 17 [*Erratum ibid.* **B 593** (2001) 731] [hep-ph/0002108] [INSPIRE].

[49] M. Freund, *Analytic approximations for three neutrino oscillation parameters and probabilities in matter*, *Phys. Rev.* **D 64** (2001) 053003 [hep-ph/0103300] [INSPIRE].

[50] M.V. Diwan et al., *Very long baseline neutrino oscillation experiments for precise measurements of mixing parameters and CP-violating effects*, *Phys. Rev.* **D 68** (2003) 012002 [hep-ph/0303081] [INSPIRE].

[51] V. Barger et al., *Precision physics with a wide band super neutrino beam*, *Phys. Rev.* **D 74** (2006) 073004 [hep-ph/0607177] [INSPIRE].

[52] V. Barger et al., *Report of the US long baseline neutrino experiment study*, arXiv:0705.4396 [INSPIRE].

[53] P. Huber and J. Kopp, *Two experiments for the price of one? — The role of the second oscillation maximum in long baseline neutrino experiments*, *JHEP* **03** (2011) 013 [*Erratum ibid.* **05** (2011) 024] [arXiv:1010.3706] [INSPIRE].

[54] M. Ghosh, S. Goswami and S.K. Raut, *Maximizing the DUNE early physics output with current experiments*, *Eur. Phys. J.* **C 76** (2016) 114 [arXiv:1412.1744] [INSPIRE].

[55] P. Coloma and E. Fernandez-Martinez, *Optimization of neutrino oscillation facilities for large θ_{13}*, *JHEP* **04** (2012) 089 [arXiv:1110.4583] [INSPIRE].

[56] ESSnuSB collaboration, E. Baussan et al., *A very intense neutrino super beam experiment for leptonic CP-violation discovery based on the European spallation source linac*, *Nucl. Phys.* **B 885** (2014) 127 [arXiv:1309.7022] [INSPIRE].

[57] S.K. Agarwalla, S. Choubey and S. Prakash, *Probing neutrino oscillation parameters using high power superbeam from ESS*, *JHEP* **12** (2014) 020 [arXiv:1406.2219] [INSPIRE].

[58] M. Blennow, P. Coloma, P. Huber and T. Schwetz, *Quantifying the sensitivity of oscillation experiments to the neutrino mass ordering*, *JHEP* **03** (2014) 028 [arXiv:1311.1822] [INSPIRE].

[59] D.V. Forero, M. Tortola and J.W.F. Valle, *Neutrino oscillations refitted*, *Phys. Rev.* **D 90** (2014) 093006 [arXiv:1405.7540] [INSPIRE].

[60] F. Capozzi, G.L. Fogli, E. Lisi, A. Marrone, D. Montanino and A. Palazzo, *Status of three-neutrino oscillation parameters, circa 2013*, *Phys. Rev.* **D 89** (2014) 093018 [arXiv:1312.2878] [INSPIRE].

[61] T. Schwetz, *What is the probability that theta(13) and CP-violation will be discovered in future neutrino oscillation experiments?*, *Phys. Lett.* **B 648** (2007) 54 [hep-ph/0612223] [INSPIRE].

[62] M. Blennow, P. Coloma and E. Fernandez-Martinez, *Reassessing the sensitivity to leptonic CP-violation*, *JHEP* **03** (2015) 005 [arXiv:1407.3274] [INSPIRE].

[63] J. Elevant and T. Schwetz, *On the determination of the leptonic CP phase*, *JHEP* **09** (2015) 016 [arXiv:1506.07685] [INSPIRE].

[64] P. Coloma, A. Donini, E. Fernandez-Martinez and P. Hernández, *Precision on leptonic mixing parameters at future neutrino oscillation experiments*, *JHEP* **06** (2012) 073 [arXiv:1203.5651] [INSPIRE].